JACS
JOURNAL OF THE AMERICAN CHEMICAL SOCIETY

Communication

pubs.acs.org/JACS

Intrinsic Relationship between Enhanced Oxygen Reduction Reaction Activity and Nanoscale Work Function of Doped Carbons

Jae Yeong Cheon,[†,⊥] Jong Hun Kim,[§,∥,⊥] Jae Hyung Kim,[‡] Kalyan C. Goddeti,[§,∥] Jeong Young Park,*[,§,∥] and Sang Hoon Joo*[,†,‡]

[†]Department of Chemistry and [‡]School of Energy and Chemical Engineering and KIER-UNIST Advanced Center for Energy, Ulsan National Institute of Science and Technology, 50 UNIST-gil, Ulsan 689-798, Republic of Korea

[§]Center for Nanomaterials and Chemical Reactions, Institute for Basic Science, Daejeon 305-701, Republic of Korea

[∥]Graduate School of EEWS, Korea Advanced Institute of Science and Technology, Daejeon 305-701, Republic of Korea

Supporting Information

ABSTRACT: Nanostructured carbon materials doped with a variety of heteroatoms have shown promising electrocatalytic activity in the oxygen reduction reaction (ORR). However, understanding of the working principles that underpin the superior ORR activity observed with doped nanocarbons is still limited to predictions based on theoretical calculations. Herein, we demonstrate, for the first time, that the enhanced ORR activity in doped nanocarbons can be correlated with the variation in their nanoscale work function. A series of doped ordered mesoporous carbons (OMCs) were prepared using N, S, and O as dopants; the triple-doped, N,S,O-OMC displayed superior ORR activity and four-electron selectivity compared to the dual-doped (N,O-OMC and S,O-OMC) and the monodoped (O-OMC) OMCs. Significantly, the work functions of these heteroatom-doped OMCs, measured by Kelvin probe force microscopy, display a strong correlation with the activity and reaction kinetics for the ORR. This unprecedented experimental insight can be used to provide an explanation for the enhanced ORR activity of heteroatom-doped carbon materials.

The oxygen reduction reaction (ORR) is a key process in clean energy technologies, such as polymer electrolyte fuel cells (PEFCs)[1] and metal−air batteries.[2] The state of the art electrocatalysts used in the ORR predominantly rely on platinum-based catalysts to overcome the sluggish reaction kinetics of the ORR.[3] However, the high cost and scarcity of platinum, as well as its susceptibility to poisoning and declining activity with use, are major drawbacks for the extensive deployment of these energy conversion devices. Therefore, a great deal of research has been devoted to developing nonprecious metal-based[4] or metal-free[5] catalysts as potential replacements for the Pt-based catalysts. In particular, since Dai et al. reported a very high ORR activity for nitrogen-doped carbon nanotubes (CNTs),[6a] metal-free ORR catalysts based on heteroatom-doped carbon nanostructures have seen remarkable progress during the past few years. Recent studies have demonstrated that the doping of heteroatoms into nanostructured carbons can give rise to an enhanced performance in the ORR in terms of both activity and reaction kinetics, when compared with their undoped analogues.[6,7] In addition, multiple-dopants-incorporated nanocarbons showed further improvement in the ORR performances.[8] In efforts to elucidate the promotion effects of dopants in the ORR, it was suggested that changes in the charge and spin densities of the carbon lattice are major factors for the enhanced performance observed with doped nanocarbons;[6a,e,7a,c,e,8b,c,e,f,9] however, these suggestions are based entirely on theoretical calculations. Experimental studies that can systemically correlate the impact of heteroatom doping in nanocarbons with enhanced ORR activity are rare.

Herein, we report direct experimental evidence that the nanoscale work function of doped nanocarbons, measured by Kelvin probe force microscopy (KPFM), is strongly correlated with the ORR activity and reaction kinetics of doped nanocarbon catalysts. We prepared a set of catalysts based on ordered mesoporous carbons (OMCs), which were selectively doped with N, S, and O. The triple-doped N,S,O-OMC exhibited superior catalytic activity and reaction kinetics in the ORR in an alkaline medium, when compared with the dual-doped (N,O-OMC and S,O-OMC) and the monodoped (O-OMC) OMC catalysts. Using surface-sensitive KPFM measurements, we demonstrate that the reactivity trend of the OMCs in the ORR can be intrinsically correlated with the work functions of the respective catalysts. Therefore, if the local work function of the OMCs can be lowered in the presence of dopants, it is possible to boost the ORR, suggesting new evidence of enhanced ORR activity associated with heteroatom doping.

Heteroatom-doped OMCs with hexagonal mesostructures were prepared via a nanocasting method using SBA-15 mesoporous silica as a template and N-, S-, and O-containing carbon sources as precursors (see the Supporting Information for details). Glucosamine, *p*-toluenesulfonic acid, and sucrose were used as sources of carbon as well as dopants. For the preparation of the triple-doped N,S,O-OMC, a mixture of glucosamine and *p*-toluenesulfonic acid was infiltrated into the SBA-15 template and carbonized at 900 °C under an inert atmosphere, followed by the removal of the SBA-15 template using HF. The dual-doped OMCs, N,O-OMC and S,O-OMC, were prepared from a mixture of glucosamine and sucrose and *p*-toluenesulfonic acid

Received: April 10, 2014
Published: June 9, 2014

   dx.doi.org/10.1021/ja503557x | J. Am. Chem. Soc. 2014, 136, 8875−8878

and sucrose, respectively. Monodoped O-OMC was produced from sucrose under similar conditions. It should be noted that while earlier literature generally neglected the role of oxygen as a dopant, there is currently an increasing notion that oxygen can modify the catalytic activity of nanocarbons.[5d,6g,7e] For comparison, the nearly dopant-free OMC was prepared using a mesophase pitch.

Scanning and transmission electron microscope (SEM and TEM, respectively) images revealed that the silica template, SBA-15 was successfully replicated onto the doped OMCs while preserving its morphology (Figures 1a,b and S1−S3). The well-

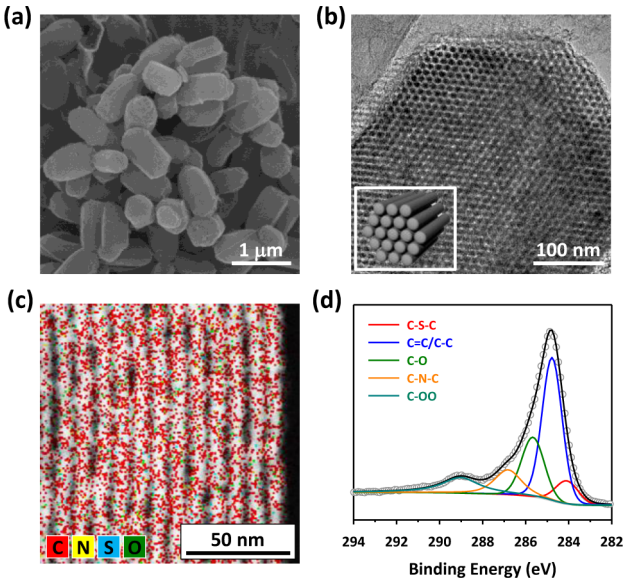

Figure 1. Characterization of the N,S,O-OMC. (a) SEM and (b) TEM images taken parallel to the pore direction. (c) HAADF-STEM image overlapped with the corresponding C, N, S, and O elemental mappings. (d) XPS C 1s spectrum.

resolved small-angle XRD peaks of the doped OMCs (Figure S4) indicated a CMK-3-type two-dimensional, hexagonally ordered mesostructure.[10] Nitrogen physisorption analysis revealed that the N,S,O-OMC has a uniform mesopore centered at ∼9.6 nm with a high Brunauer−Emmett−Teller (BET) surface area (1060 $cm^2 g^{-1}$) and total pore volume of 1.85 $cm^3 g^{-1}$. The other doped OMCs also showed high BET surface areas and pore volumes, similar to those found with the N,S,O-OMC (Figure S5 and Table S1). The presence of dopants in the N,S,O-OMC was confirmed by using high angle annular dark-field scanning TEM (HAADF STEM) image coupled with the elemental mapping image of the respective elements (Figures 1c and S6). The incorporation of dopants in the other OMC samples was also confirmed by elemental mapping images (Figure S7−S9). X-ray photoelectron spectroscopy (XPS) was used to further investigate the chemical nature of the heteroatoms in the N,S,O-OMC as well as other doped OMCs (Figures 1d and S10−S13). The high-resolution XPS C 1s spectrum of the N,S,O-OMC (Figure 1d) was highly asymmetric because of the presence of C−C and C═C bonds as well as heteroatom-containing bonding moieties. The deconvolution of the C 1s peak includes the C−S−C (284.1 eV), C−C/C═C (284.8 eV), C−O (285.6 eV), and C−N−C (286.8 eV) bonding moieties, which indicates that the N, S, and O dopants were successfully incorporated into the carbon framework of the N,S,O-OMC (Figure 1d).[8c] The O-OMC (Figure S11), N,O-OMC (Figure S12), and S,O-OMC (Figure S13) catalysts also showed similar XPS spectra to those of the N,S,O-OMC. The nearly dopant-free OMC (Figure S14) contained oxygen, but its O-content was very low, when compared with that found in the O-OMC. The details of the chemical composition of the doped and undoped OMCs are summarized in Table S2. Overall, a series of five OMCs with similar textural properties bearing different types of dopant have been prepared and can be used as model catalysts for the systematic investigation of the dopant effects in the ORR.

To investigate the electrocatalytic activity of the heteroatom-doped OMCs in the ORR, linear sweep voltammetry (LSV) experiments were performed on a rotating ring disk electrode (RRDE) using an O_2-saturated solution of 0.1 M KOH, at a scan rate of 5 mV s^{-1} and a rotating speed of 1600 rpm (Figure 2a,

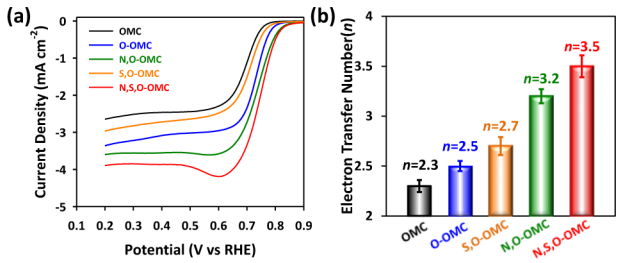

Figure 2. (a) LSV curves of the doped OMCs for the ORR. (b) Electron-transfer numbers of the doped OMCs at 0.6 V (vs RHE) during the ORR.

S15−16, and Table S3). As a benchmark, the LSV curve of a Pt/C catalyst was displayed with those of the doped OMCs in Figure S17. Among the investigated samples, the OMC displayed the lowest ORR activity in terms of on-set and half-wave potentials. The monodoped O-OMC showed enhanced ORR activity, when compared to the OMC, indicating the beneficial effect of oxygen atoms in the ORR. The dual doping of N and O in N,O-OMC resulted in higher ORR activity when compared to the O-OMC. However, the sulfur and oxygen dual-doped S,O-OMC exhibited a lower ORR activity than that found with O-OMC. It is known that electronegative N atoms (3.04) break the charge neutrality of C atoms (2.55) atoms in the sp^2 carbon lattice, providing adsorption sites for oxygen moelcules.[6a] On the other hand, sulfur atoms (2.58) have an electronegativity similar to that of carbon atoms (2.55) and the effect of sulfur doping on the ORR is still controversial.[5d,7e] Similar to our results, Qiao et al. reported that S-doped graphene has a higher adsorption free energy of the ORR intermediate (OOH) compared to that of O-doped graphene, resulting in lower ORR activity.[7e] Finally, triple-doped N,S,O-OMC exhibited a further enhancement in ORR activity when compared to N,O-OMC, which makes the N,S,O-OMC the most active catalyst among the doped OMCs prepared in this study. The most active N,S,O-OMC showed an on-set potential at 0.85 V, and its kinetic current density at 0.75 V was 3.8 mA cm^{-2}. The enhanced ORR activity of the N,S,O-OMC catalyst is consistent with those previously reported.[8c,d,g]

To gain further insight into the role of heteroatom doping in carbon, we investigated the reaction kinetics using the RRDE method. The H_2O_2 yields (Figure S18) were calculated by measuring the ring current, from which the number of electrons (n) transferred during the ORR could be obtained (Figure 2b and Table S3). The O-OMC had an n value of 2.5 at 0.6 V, suggesting that its oxygen reduction proceeds via a quasi-two-electron process. Note that the participation of a surface quinone group of oxygen functionalized carbon during the reduction of

dx.doi.org/10.1021/ja503557x | J. Am. Chem. Soc. 2014, 136, 8875−8878

O_2 often leads to the peroxide pathway.[5d] On the other hand, N or S doping to nanostructured carbon was found to convert the ORR activity from a two- to a four-electron reduction pathway.[6e,7c] In addition, the enhanced four-electron selectivity was also observed in the dual-doped OMC catalysts. The *n* values for the dual-doped N,O-OMC and S,O-OMC were 3.2 and 2.7, respectively. Triple-doped N,S,O-OMC displayed an increased *n* value of 3.5, which indicates that the ORR over the N,S,O-OMC proceeds via a quasi-four-electron pathway. This result suggests that triple doping with N, S, and O in the OMC has a synergistic impact on the ORR activity and selectivity, giving rise to enhanced performance when compared to the dual- and monodoped OMCs.

The experimental results presented in this work as well as in previously reported studies[5−8] clearly suggest that heteroatom doping in carbon lattices can provide enhanced ORR activity and reaction kinetics. Dai et al. substantiated this phenomenon by density functional theory (DFT) calculations; they showed that the high electron affinity of N in N-doped carbon nanotubes can induce a positive charge density on an adjacent C atom, which can facilitate oxygen adsorption and subsequently weaken the bonding in the oxygen molecule.[6a] For the dual-doped system, Qiao et al. suggested using DFT calculations that N and S dual-doped graphene induces an upshift of its maximum spin density, which results in a significantly enhanced ORR activity.[8c] Luo et al. showed the enhanced ORR activity of N-doped graphene was associated with the reduced work function due to an increase in the density of π states near the Fermi level using ultraviolet photoemission spectroscopy.[11]

In our study, the local work function of doped OMC was characterized using KPFM to understand the correlation between ORR activity and the variation in work function and to address the role of the dopants in the enhancement of the ORR activity. KPFM is a derivative imaging mode of scanning probe microscopy and is a versatile technique that can directly monitor the changes in local work function of solid surfaces with an energy resolution of at ∼10 mV, together with the corresponding topography. Because KPFM measures the voltage required to nullify the work function difference between the conductive tip and the sample ($\varphi_{tip} - \varphi_{sample}$), the contrast in the contact potential difference (CPD) image is equivalent to the local work function variation of the sample.[12] KPFM has been widely used to investigate the influence of dopants or atomic scale defects on the variation of work function.[12]

KPFM measurements on the OMC surfaces were carried out using an Agilent 5500 atomic force microscope (AFM) with a conductive noncontact cantilever coated with Pt/Ir and a nominal resonance frequency of 75 kHz. For the CPD measurement, samples were prepared by transferring the OMCs onto a gold-coated silicon wafer using a drop-casting method. Because the OMC partially covers the gold substrate, the measured CPD value on gold substrates can be used as the reference value. Therefore, the work function of various doped OMCs can be determined at a nanometer scale without any ambiguity. SEM was used to monitor the overall distributions of the OMCs as shown in Figure S19.

Figure 3a,b shows the topographical and CPD images simultaneously taken on the O-OMC, respectively. Figure 3c shows the line profiles acquired along the white dashed lines of the O-OMC sample. The height of the O-OMC was typically 100−200 nm. The dark contrast observed in the CPD image indicates a high sample work function, therefore the φ of the O-OMC is higher than that of the gold plate by ∼50 mV (Figure 3c). Considering that φ_{Au} and φ_{carbon} are reported as 4.9−5[13] and ∼5 eV,[14] respectively, the measured value of the work function on the OMC is consistent with those previously reported. However, the CPD images of N,S,O-OMC clearly show a different contrast, as shown in the topographical (Figure 3d) and CPD images (Figure 3e). Figure 3f shows the line profile of the topographical and CPD images acquired along the white dashed lines for the N,S,O-OMC sample. As shown in Figure 3e,f, the triple-doped N,S,O-OMC displays a bright contrast indicating a lower work function than observed with φ_{Au} of ∼70 mV.

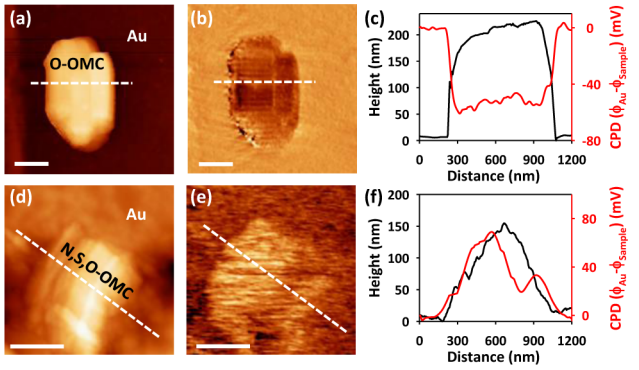

Figure 3. (a,d) Topography and (b,e) CPD images for the O-OMC (top) and the N,S,O-OMC (bottom). The scale bar at the bottom left of the figures is 400 nm. For both samples, the height and CPD profiles along the white dashed lines are drawn in (c) and (f) as the black and the red lines, respectively.

To increase the reproducibility and ascertain the correlation with the ORR activity tests, CPD measurements were carried out on the multiple OMC particles placed at various locations (Figure 4a). The error bar in Figure 4a represents the standard deviation associated with the multiple measurements on five different samples, and the insets show representative CPD maps for each sample (Figure S20 shows the corresponding topography images). Figure 4a shows a plot of the CPD measured on

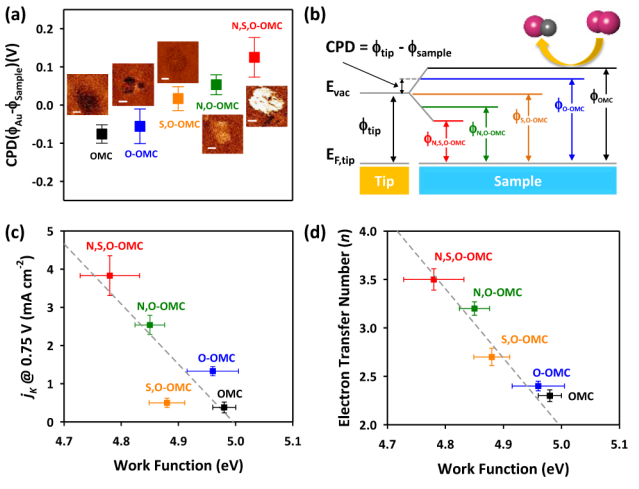

Figure 4. (a) CPD variation depending on the OMC dopants (insets: representative CPD images for each specimen using a common CPD scale; scale bar is 200 nm). (b) Energy diagram of the tip−sample system where oxygen reduction can be activated when an electron overcomes the potential barrier of the work function. E_{vac} implies the vacuum level. For each sample, the colors for the work function notation in (b) match those in (a). (c,d) Correlation of ORR activity (c) and four-electron selectivity (d) of the doped OMCs with their work function values.

dx.doi.org/10.1021/ja503557x | J. Am. Chem. Soc. 2014, 136, 8875−8878

OMC, O-OMC, S,O-OMC, N,O-OMC, and N,S,O-OMC, which clearly reveals a systematic variation of CPD values (and therefore their work functions) depending on the type of dopants used. The CPD images of the samples (Figure 4a, inset) exhibit gradual changes from the darkest contrast found in the OMC to the brightest contrast found in the N,S,O-OMC, in accordance with changes in the CPD values. This systematic change in work functions of the samples is depicted in the energy diagram of the tip−sample systems shown in Figure 4b.

The work functions of the doped OMCs were correlated with their kinetic current densities at 0.75 V (Figure 4c) and with their electron-transfer numbers (n) during the ORR (Figure 4d). Figure 4c,d indicates that these kinetic parameters are inversely proportional to the work functions of each sample. In particular, the n values of the doped OMCs have a strong linear relationship with their work function. This indicates that a sample with a lower work function (i.e., higher CPD value) has a lower energetic barrier for donating electrons from the surface of the catalyst to the adsorbed oxygen, thereby facilitating the formation of the OOH species, which is known to be the rate-determining step in the ORR.[7e] We also measured the ORR activity of the doped OMCs in an acidic medium (0.1 M $HClO_4$) and correlated the ORR reactivity with the work function values (Figure S21). We found that the LSV curves of the doped OMCs in acid showed the same trend as those in alkaline solutions. In addition, the correlation between the ORR activity and kinetics of the doped OMCs in acid with their work functions exhibited the same trends as those measured in alkaline solutions, confirming that the work function of a carbon-based catalyst can be used as an effective parameter for predicting the ORR activity.

In conclusion, we prepared a series of heteroatom-doped OMCs as metal-free electrocatalysts for a systematic study into the dopant effects in the ORR. The triple-doped N,S,O-OMC catalyst displayed the best ORR activity and four-electron selectivity, when compared to the dual-doped (N,O- and S,O-OMC) and monodoped (O-OMC) OMC catalysts. KPFM was used to investigate the doped OMCs, and their work function was found to be dependent on the type of dopant used. Significantly, we established that the nanoscale work function of the doped OMCs, measured by KPFM, could be correlated with their ORR activity and reaction kinetics. We envisage from this unprecedented insight that the work function of the doped nanocarbons can be generally used as an activity descriptor for the ORR as well as other catalytic reactions. In addition, this study may provide the design principle for the development of advanced electrocatalysts for other important reactions.

■ ASSOCIATED CONTENT

Supporting Information

Experimental details and related references. This material is available free of charge via the Internet at http://pubs.acs.org.

■ AUTHOR INFORMATION

Corresponding Author

shjoo@unist.ac.kr; jeongypark@kaist.ac.kr

Author Contributions

⊥Jae Yeong Cheon and Jong Hun Kim contributed equally to this work.

Notes

The authors declare no competing financial interest.

■ ACKNOWLEDGMENTS

This work was supported by the National Research Foundation of Korea (NRF-2013R1A1A2012960), the New and Renewable Energy Core Technology Program of the KETEP funded by the MTIE (20133030011320), and the Institute for Basic Science (IBS) [CA1401-04], Republic of Korea. J.Y.C. acknowledges the National Junior Research Fellowship (NRF-2013H1A8A1003741).

■ REFERENCES

(1) (a) Steele, B. C. H.; Heinzel, A. *Nature* **2001**, *414*, 345. (b) Debe, M. K. *Nature* **2012**, *486*, 43.

(2) Bruce, P. G.; Freunberger, S. A.; Hardwick, L. J.; Tarascon, J. M. *Nat. Mater.* **2012**, *11*, 19.

(3) Gasteiger, H. A.; Kocha, S. S.; Sompalli, B.; Wagner, F. T. *Appl. Catal., B* **2005**, *56*, 9.

(4) (a) Lefevre, M.; Proietti, E.; Jaouen, F.; Dodelet, J.-P. *Science* **2009**, *324*, 71. (b) Wu, G.; More, K. L.; Johnston, C. M.; Zelenay, P. *Science* **2011**, *332*, 443. (c) Cheon, J. Y.; Kim, T.; Choi, Y.; Jeong, H. Y.; Kim, M. G.; Sa, Y. J.; Kim, J.; Lee, Z.; Yang, T. H.; Kwon, K.; Terasaki, O.; Park, G. G.; Adzic, R. R.; Joo, S. H. *Sci. Rep.* **2013**, *3*, 2715.

(5) (a) Zheng, Y.; Jiao, Y.; Jaroniec, M.; Jin, Y.; Qiao, S. Z. *Small* **2012**, *8*, 3550. (b) Dai, L. *Acc. Chem. Res.* **2013**, *46*, 31. (c) Paraknowitsch, J. P.; Thomas, A. *Energy Environ. Sci.* **2013**, *6*, 2839. (d) Wang, D.-W.; Su, D. *Energy Environ. Sci.* **2014**, *7*, 576.

(6) (a) Gong, K.; Du, F.; Xia, Z.; Durstock, M.; Dai, L. *Science* **2009**, *323*, 760. (b) Liu, R.; Wu, D.; Feng, X.; Müllen, K. *Angew. Chem., Int. Ed.* **2010**, *49*, 2565. (c) Qu, L.; Liu, Y.; Baek, J.-B.; Dai, L. *ACS Nano* **2010**, *3*, 1321. (d) Yang, S.; Feng, X.; Wang, X.; Müllen, K. *Angew. Chem., Int. Ed.* **2011**, *50*, 5339. (e) Zheng, Y.; Jiao, Y.; Chen, J.; Liu, J.; Liang, J.; Du, A.; Zhang, W.; Zhu, Z.; Smith, S. C.; Jaroniec, M.; Lu, G. Q.; Qiao, S. Z. *J. Am. Chem. Soc.* **2011**, *133*, 20116. (f) Kwon, K.; Sa, Y. J.; Cheon, J. Y.; Joo, S. H. *Langmuir* **2012**, *28*, 991. (g) Silva, R.; Voiry, D.; Chhowalla, M.; Asefa, T. *J. Am. Chem. Soc.* **2013**, *135*, 7823.

(7) (a) Yang, L.; Jiang, S.; Zhao, Y.; Zhu, L.; Chen, S.; Wang, X.; Wu, Q.; Ma, J.; Ma, Y.; Hu, Z. *Angew. Chem., Int. Ed.* **2011**, *50*, 7132. (b) Yang, S. B.; Zhi, L. J.; Tang, K.; Feng, X.; Maier, J.; Müllen, K. *Adv. Funct. Mater.* **2012**, *22*, 3634. (c) Jeon, I.-Y.; Zhang, S.; Zhang, L.; Choi, H.-J.; Seo, J.-M.; Xia, Z.; Dai, L.; Baek, J.-B. *Adv. Mater.* **2013**, *25*, 6138. (d) Yang, D.; Bhattacharjya, D.; Inamdar, S.; Park, J.; Yu, J. S. *J. Am. Chem. Soc.* **2012**, *134*, 16127. (e) Jiao, Y.; Zheng, Y.; Jaroniec, M.; Qiao, S. Z. *J. Am. Chem. Soc.* **2014**, *136*, 4394.

(8) (a) Wang, S.; Iyyamperumal, E.; Roy, A.; Xue, Y.; Yu, D.; Dai, L. *Angew. Chem., Int. Ed.* **2011**, *50*, 11756. (b) Wang, S.; Zhang, L.; Xia, Z.; Roy, A.; Chang, D. W.; Baek, J. B.; Dai, L. *Angew. Chem., Int. Ed.* **2012**, *51*, 4209. (c) Liang, J.; Jiao, Y.; Jaroniec, M.; Qiao, S. Z. *Angew. Chem., Int. Ed.* **2012**, *51*, 11496. (d) Liu, X.; Antonietti, M. *Adv. Mater.* **2013**, *25*, 6284. (e) Zheng, Y.; Jiao, Y.; Ge, L.; Jaroniec, M.; Qiao, S. Z. *Angew. Chem., Int. Ed.* **2013**, *52*, 3110. (f) Zhao, Y.; Yang, L.; Chen, S.; Wang, X.; Ma, Y.; Wu, Q.; Jiang, Y.; Qian, W.; Hu, Z. *J. Am. Chem. Soc.* **2013**, *135*, 1201. (g) Xu, J.; Dong, G.; Jin, C.; Huang, M.; Guan, L. *ChemSusChem* **2013**, *6*, 493.

(9) Zhang, L.; Xia, Z. *J. Phys. Chem. C* **2011**, *115*, 11170.

(10) Jun, S.; Joo, S. H.; Ryoo, R.; Kruk, M.; Jaroniec, M.; Liu, Z.; Ohsuna, T.; Terasaki, O. *J. Am. Chem. Soc.* **2000**, *122*, 10712.

(11) Luo, Z.; Lim, S.; Tian, Z.; Shang, J.; Lai, L.; MacDonald, B.; Fu, C.; Shen, Z.; Yu, T.; Lin, J. *J. Mater. Chem.* **2011**, *21*, 8038.

(12) (a) Liscio, A.; Palermo, V.; Samori, P. *Acc. Chem. Res.* **2010**, *43*, 541. (b) Liu, C.; Hwang, Y. J.; Jeong, H. E.; Yang, P. *Nano Lett.* **2011**, *11*, 3755. (c) Kim, J.-H.; Hwang, J. H.; Suh, J.; Tongay, S.; Kwon, S.; Hwang, C. C.; Wu, J.; Park, J. Y. *Appl. Phys. Lett.* **2013**, *103*, 171604.

(13) (a) de Boer, B.; Hadipour, A.; Mandoc, M. M.; van Woudenbergh, T.; Blom, P. W. M. *Adv. Mater.* **2005**, *17*, 621. (b) Ravirajan, P.; Haque, S. A.; Durrant, J. R.; Poplavskyy, D.; Bradley, D. D. C.; Nelson, J. *J. Appl. Phys.* **2004**, *95*, 1473.

(14) (a) de Jonge, N.; Allioux, M.; Doytcheva, M.; Kaiser, M.; Teo, K. B. K.; Lacerda, R. G.; Milne, W. I. *Appl. Phys. Lett.* **2004**, *85*, 1607. (b) Gao, R. P.; Pan, Z. W.; Wang, Z. L. *Appl. Phys. Lett.* **2001**, *78*, 1757.